

Turbo Coded and Cooperative Network Coded Non-Coherent Soft-Decision Star-QAM Dispensing with Channel Estimation

Dandan Liang, Meng Song, Soon Xin Ng and Lajos Hanzo
 School of ECS, University of Southampton, SO17 1BJ, United Kingdom.
 Email: {dl4e08, ms6e09, sxn, lh}@ecs.soton.ac.uk.

Abstract—Star Quadrature Amplitude Modulation (Star-QAM) is a non-coherent detection aided scheme ideal for low-complexity wireless transceivers. In this contribution, we first derive soft-decision aided StQAM symbol-to-bit demapping combined with iterative detection aided Turbo Coding (TC). Then we combine this physical layer design with network coding (NC) and quantify the attainable coding gain. It is shown that the proposed 16-level Star-QAM (16-StQAM) based TC scheme is capable of achieving a coding gain of about 1.5 dB over the TC aided 16-level Differential Phase-Shift Keying (16DPSK) benchmark scheme at a BER of 10^{-5} . The 16-StQAM based TC assisted scheme is capable of offering another 1.2 dB coding gain, when it is employed in a 'butterfly' topology network arrangement. When the source and relay nodes are allowed to transmit at different power levels, the two-hop 16-StQAM based TC aided NC scheme outperforms the single-hop 16-StQAM based TC scheme by approximately 2.2 dB.

I. INTRODUCTION

Coherent detection aided Quadrature Amplitude Modulation (QAM) requires accurate Channel State Information (CSI) in order to avoid false-phase locking, especially when communicating over Rayleigh fading channels [1]–[3]. As a remedy, differentially detected non-coherent Star-QAM (StQAM) was proposed in [4] in order to dispense with high-complexity CSI estimation. Operating without CSI is of particular importance in the context of relay-aided NC assisted systems, where the relay nodes (RN) cannot be realistically expected to estimate all the channels invoked. More specifically, 16-level Star-QAM (16-StQAM) is based on two concentric 8-level Phase-Shift Keying (8PSK) constellations having two different amplitudes. StQAM schemes having more than two PSK constellations are also referred to as Differential Amplitude and Phase-Shift Keying (DAPSK) schemes [5], [6]. The authors of [5], [6] have further improved the performance of DAPSK/StQAM schemes [5], [6]. However, despite its attractive performance versus complexity characteristics, soft-decision based demodulation has not been conceived for these StQAM and DAPSK schemes. This also implies that without soft-decision based demodulation, the potential power of sophisticated channel coding or coded modulation schemes cannot be fully exploited. Hence, when channel coding was incorporated into StQAM as in [4], its performance was far from the channel capacity due to the employment of hard-decision rather than soft-decision based demodulation. Soft-decision assisted StQAM was designed for Iteratively Detected Bit-Interleaved Coded Modulation (BICM-ID) in [7]. As a further improvement, Turbo Coding (TC) [8] is adopted in this contribution because its EXIT curve was found to have a better match with that of the 16-StQAM demapper. Furthermore, this improved physical layer design is combined with network coding (NC) in our paper. Both NC [9] and cooperative communications [10], [11] have recently been widely researched. In a cooperative communication scheme, RNs are used to forward signals received from other users to the destination nodes (DN). By contrast,

The research leading to these results has received funding from the European Union's Seventh Framework Programme (FP7/2007-2013) under grant agreement no (214625). The financial support of the RC-UK IU-ATC and that of the China-UK Science Bridge in 4G wireless communications is also gratefully acknowledged.

a NC scheme allows RNs to combine the information received from different information source nodes (SN) before broadcasting them to various DNs. In this contribution, we consider a 'butterfly' topology based NC scheme [12], where two SNs and two DNs are assisted by a single RN. Our novel contributions are as follows:

- 1) First, we derive the Log-Likelihood Ratio (LLR) [13] formula for the soft-decision demodulation of 16-StQAM. Then the performance benefits of using this new formula will be quantified in the context of a TC [8] aided 16-StQAM scheme, when communicating over correlated Rayleigh fading channels. Note, however that the proposed soft-decision based 16-StQAM demodulation principles may be readily extended to DAPSK schemes having more than two concentric PSK constellations.
- 2) Finally, we employ the 16-StQAM aided TC based physical layer scheme for assisting a butterfly topology based NC system. A power sharing mechanism is also proposed for further reducing the overall transmit power requirement of the network.

The outline of the paper is as follows. Our system model is described in Section II, while our results and discussions are detailed in Section III. Our conclusions are presented in Section IV.

II. SYSTEM MODEL AND ANALYSIS

A. Star-QAM Mapper and Soft-Decision Demapper Aided TC

1) *Star-QAM Mapper*: As seen in Fig. 1, the 16-StQAM mapper consists of three components, namely the amplitude selector, the 8PSK mapper and a differential encoder as detailed in Chapter 11 of [2]. The 8PSK mapper and the differential encoder jointly form a conventional 8-level DPSK (8DPSK) mapper. The Most Significant Bit (MSB) of the BICM-encoded symbol, namely b_3 , is used for selecting one of the two possible amplitudes. More specifically, b_3 , is used for selecting the amplitude of the PSK ring, a_k . The two possible amplitude values are denoted as $a^{(1)}$ and $a^{(2)}$, respectively. When the MSB of the k th TC symbol is given by $b_3 = 0$, the amplitude of the PSK ring will remain the same as that of the previous value, yielding $a_k = a_{k-1}$. By contrast, the amplitude of the PSK ring will be switched to the other legitimate value, if $b_3 = 1$. This amplitude selection mechanism may be referred to as 2-level Differential Amplitude Shift Keying (2DASK). After normalisation for the sake of maintaining a symbol energy of unity, we have $a^{(1)} = 1/\sqrt{2.5}$ and $a^{(2)} = 2/\sqrt{2.5}$. The amplitude value of the reference symbol is given by $a_0 = a^{(1)}$. The remaining 3 bits, namely b_2 b_1 b_0 , are used by the 8DPSK mapper. Note that similarly to any DPSK scheme, we insert a reference symbol at the beginning of each frame in front of the 16-StQAM mapper of Fig. 1.

The k th differentially encoded symbol v_k can be expressed as:

$$v_k = v_{k-1} w_k, \quad (1)$$

where $w_k = \mu(b_2 b_1 b_0)$ is the k th 8PSK symbol based on the 8PSK mapper function of $\mu(\cdot)$, while v_{k-1} is the $(k-1)$ th 8DPSK symbol and $|v_k|^2 = 1$. The reference symbol for the 8DPSK part is given

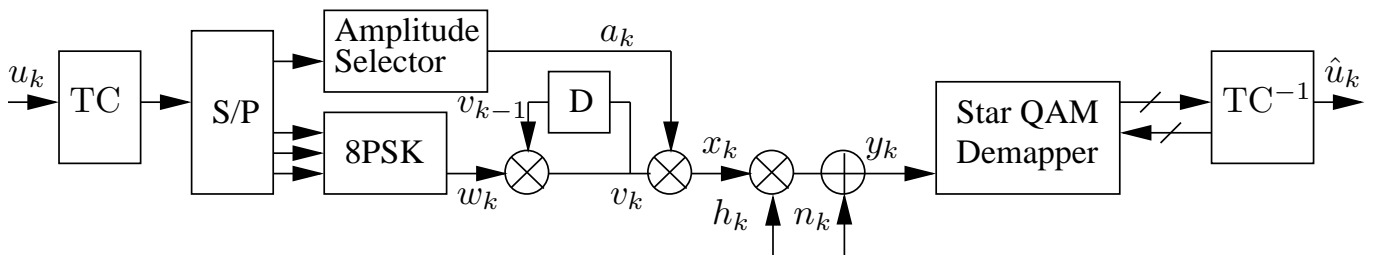


Fig. 1. The schematic of one link system employing 16-level star-QAM aided TC scheme. The interleavers and de-interleavers between the encoder/decoder and mapper/demapper are not presented for simplicity.

by $v_0 = \mu(0 \ 0 \ 0)$. The k th 16-StQAM symbol is given by:

$$x_k = a_k v_k, \quad (2)$$

where $a_k \in \{a^{(1)}, a^{(2)}\}$.

2) *Star-QAM Soft Demapper*: The soft-decision based Star-QAM detector is shown in front of the TC decoder (TC^{-1}) of Fig. 1, where the k th received symbol can be written as:

$$y_k = h_k x_k + n_k = h_k a_k v_k + n_k, \quad (3)$$

where h_k is the Rayleigh fading channel's coefficient, and n_k represents the AWGN having a variance of $N_0/2$ per dimension. Assuming a slowly fading Rayleigh channel, where $h_k \approx h_{k-1}$, we can rewrite (3) using (1) as:

$$\begin{aligned} y_k &= h_{k-1} a_k v_{k-1} x_k + n_k, \\ &= \frac{a_k}{a_{k-1}} y_{k-1} w_k - \frac{a_k}{a_{k-1}} n_{k-1} x_k + n_k, \\ &= p_k y_{k-1} w_k + \tilde{n}_k, \end{aligned} \quad (4)$$

where $p_k = \frac{a_k}{a_{k-1}}$ is the ratio of the k th and $(k-1)$ st amplitudes, while $\tilde{n}_k = -\frac{a_k}{a_{k-1}} n_{k-1} w_k + n_k$ is the effective noise.

Three amplitude ratios can be derived from the two PSK ring amplitudes of the 16-StQAM as follows:

$$p_k = \begin{cases} R_0 = a^{(1)}/a^{(1)} = a^{(2)}/a^{(2)} = 1 \\ R_1 = a^{(1)}/a^{(2)} \\ R_2 = a^{(2)}/a^{(1)}. \end{cases} \quad (5)$$

The noise variance of \tilde{n}_k in (4) can be computed as:

$$\tilde{N}_0 = N_0 + |p_k|^2 |w_k|^2 N_0 = N_0 (1 + |p_k|^2), \quad (6)$$

where $\tilde{N}_0 = 2N_0 = N_0^{(0)}$ if $b_3 = 0$ while $\tilde{N}_0 = (1 + R_1^2)N_0 = N_0^{(1)}$ or $\tilde{N}_0 = (1 + R_2^2)N_0 = N_0^{(2)}$ if $b_3 = 1$. Based on (4), (5) and (6), we can derive the LLR of b_0 , b_1 , b_2 and b_3 at (7) and (8), where $w^{(m)} = \mu(b_2 b_1 b_0)$ and μ is the conventional 8PSK mapper function and $P^a(b_i)$ represents the *a priori* bit probabilities, where b_i denotes the i th coded bit of the symbol and $\chi(i, b)$ is the set of constellation points having the i th bit set to b .

3) *Analysis of 16-StQAM Aided TC Scheme*: Extrinsic Information Transfer (EXIT) Charts [14]–[16] are used for analysing the 16-StQAM scheme. Fig. 2 shows the EXIT curves of two different inner codes and that of the outer TC of Fig. 1, complemented by the decoding trajectories of the 16-StQAM and 16DPSK aided TC schemes. Meanwhile, the EXIT curve of an outer convolutional code is shown as a reference. The inner code's EXIT curve recorded for our 16-StQAM symbol-to-bit demapper (the solid-straight line) has a higher starting point at $I_{A_1}=0$ than that of the 16DPSK (the dotted-straight line), although they have a similar value at $I_{A_1}=1$. Note that the area under a specific EXIT curve is related to the achievable channel capacity [14]–[16] and this area under the 16-StQAM EXIT curve is higher than that under the 16DPSK inner code's EXIT curve. Hence, the capacity of the 16-StQAM based scheme is higher than

that of the 16DPSK based scheme. Furthermore, it is also seen in Fig. 2 that the TC-aided 16-StQAM scheme requires a lower number of decoding iterations in order to achieve decoding convergence to a vanishingly low BER compared to that of the TC-aided 16DPSK scheme. It is worth noting that the EXIT curve of the convolutional decoder does not match that of the 16-StQAM demapper, while that of the TC does.

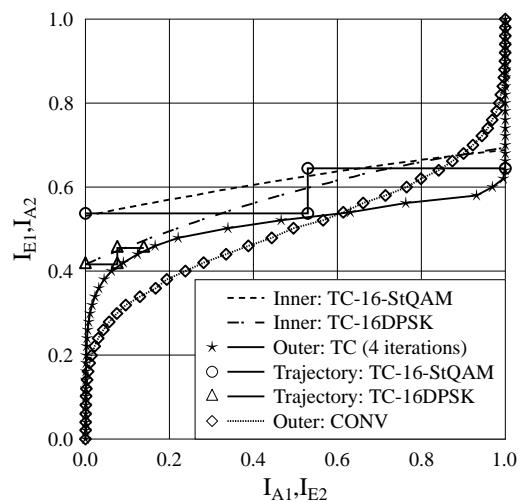


Fig. 2. EXIT Charts of 16-StQAM and 16DPSK aided TC over correlated Rayleigh channel with $E_b/N_0 = 10$ dB. The detailed simulation parameters are shown in Table. 1

B. Network Coding Model

Fig. 3 shows the NC topology used in our study. The system consists of two SNs: SN_1 and SN_2 , a RN and two DNs: DN_1 and DN_2 . During the first cooperative transmission period, the binary sequence \mathbf{b}_1 emanating from SN_1 is turbo-encoded and (16-StQAM or DPSK) modulated to generate the sequence \mathbf{x}_{s_1} , before it is transmitted to both RN and DN_2 . The estimated sequence $\hat{\mathbf{b}}_1$ is available at both RN and DN_2 after demodulation and decoding. Similarly, during the second cooperative transmission period, the binary sequence \mathbf{b}_2 emerging from SN_2 is turbo-encoded and (16-StQAM or DPSK) modulated to generate \mathbf{x}_{s_2} , before it is transmitted to both RN and DN_1 . The estimated sequence $\hat{\mathbf{b}}_2$ is available at both RN and DN_1 after demodulation and decoding. Then, RN combines both decoded information sequences with the aid of binary modulo addition as $\mathbf{b}_3 = \hat{\mathbf{b}}_1 \oplus \hat{\mathbf{b}}_2$, before it is turbo-encoded and modulated, yielding \mathbf{x}_r . In the last cooperative transmission period, \mathbf{x}_r is broadcast to both DN_1 and DN_2 . After demodulation and decoding the estimated sequence $\hat{\mathbf{b}}_3$ becomes available at both DN_1 and DN_2 . Finally, the estimate of \mathbf{b}_1 can be obtained at DN_1 with the aid of $\hat{\mathbf{b}}_1 = \hat{\mathbf{b}}_3 \oplus \hat{\mathbf{b}}_2$. Similarly, we have $\hat{\mathbf{b}}_2 = \hat{\mathbf{b}}_3 \oplus \hat{\mathbf{b}}_1$ at DN_2 . Let

$$L^e(b_i) = \frac{\sum_{w^{(m)} \in \chi(i,0)} \left(\frac{1}{\pi N_0^{(0)}} e^{-\frac{|y_k - y_{k-1} R_0 w^{(m)}|^2}{N_0^{(0)}}} + \frac{1}{\pi N_0^{(1)}} e^{-\frac{|y_k - y_{k-1} R_1 w^{(m)}|^2}{N_0^{(1)}}} + \frac{1}{\pi N_0^{(2)}} e^{-\frac{|y_k - y_{k-1} R_2 w^{(m)}|^2}{N_0^{(2)}}} \right) \prod_{j \neq i}^3 P^a(b_j)}{\sum_{w^{(m)} \in \chi(i,1)} \left(\frac{1}{\pi N_0^{(0)}} e^{-\frac{|y_k - y_{k-1} R_0 w^{(m)}|^2}{N_0^{(0)}}} + \frac{1}{\pi N_0^{(1)}} e^{-\frac{|y_k - y_{k-1} R_1 w^{(m)}|^2}{N_0^{(1)}}} + \frac{1}{\pi N_0^{(2)}} e^{-\frac{|y_k - y_{k-1} R_2 w^{(m)}|^2}{N_0^{(2)}}} \right) \prod_{j \neq i}^3 P^a(b_j)} \quad (7)$$

$$L^e(b_3) = \frac{\sum_{w^{(m)}} \text{All} \left(\frac{1}{\pi N_0^{(0)}} e^{-\frac{|y_k - y_{k-1} R_0 w^{(m)}|^2}{N_0^{(0)}}} \right) \prod_{j=0}^2 P^a(b_j)}{\sum_{w^{(m)}} \text{All} \left(\frac{1}{\pi N_0^{(1)}} e^{-\frac{|y_k - y_{k-1} R_1 w^{(m)}|^2}{N_0^{(1)}}} + \frac{1}{\pi N_0^{(2)}} e^{-\frac{|y_k - y_{k-1} R_2 w^{(m)}|^2}{N_0^{(2)}}} \right) \prod_{j=0}^2 P^a(b_j)} \quad (8)$$

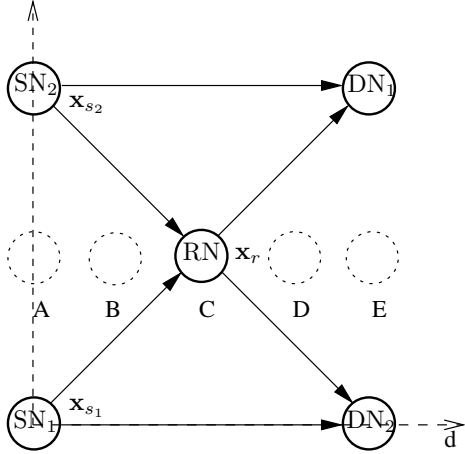


Fig. 3. The schematic of our squared butterfly network topology. A, B, C, D and E represent different RN locations which are in the centre line of SN_1 and SN_2 .

us now consider the overall throughput and the path-loss reduction factor in the following two subsections:

1) *Overall throughput of our system:* In our NC aided system, the overall throughput can be formulated as:

$$R_o = R_s \times R_c \times R_m, \quad (9)$$

where $R_s = \frac{\text{number of sources}}{\text{time slots}}$ is the overall system's normalised throughput, i.e. rate, while R_c is the coding rate and R_m is the number of bits per modulated symbol. Hence, in our proposed system we have $R_o = 2/3 \times 1/2 \times 4 = 4/3$. The throughput of a non-cooperative scheme is given by $R_o = 1/1 \times 1/2 \times 4 = 2$.

2) *Reduced-distance-related pathloss reduction (RDRPLR):* The RDRPLR of the S_1R link with respect to the S_1D_1 link can be expressed as [17], [18]:

$$G_{S_1R} = \left(\frac{d_{S_1D_1}}{d_{S_1R}} \right)^\aleph, \quad (10)$$

where the pathloss exponent equals to $\aleph = 2$, when a free-space pathloss model is assumed. Similarly, the RDRPLR of the RD_1 link in relation to the S_1D_1 link may be formulated as:

$$G_{RD_1} = \left(\frac{d_{S_1D_1}}{d_{RD_1}} \right)^2. \quad (11)$$

Naturally, the RDRPLR of the S_1D_1 link related to itself is unity, yielding, $G_{S_1D_1} = 1$, where d_{S_1R} represents the distance between SN_1 and RN, while d_{RD_1} is that of the RD_1 link and $d_{S_1D_1}$ is that of the S_1D_1 link.

From the network topology of Fig. 3, $d_{S_1D_2}$ may be calculated as:

$$d_{S_1D_2} = \frac{d_{S_1D_1}}{\sqrt{2}}. \quad (12)$$

Furthermore, the above algorithm can be used for the S_2D_2 link. When RN is located at the centre denoted as 'C' in Fig. 3, we have $G_{S_1R} = G_{RD_1} = G_{S_2R} = G_{RD_2} = 4$ (6 dB) and $G_{S_1D_2} = G_{S_2D_1} = 2$ (3 dB).

C. Power Sharing Methodology

When the RDRPLR factor between node a and node b , namely G_{ab} , as well as the transmit power of node a , namely $P_{t,a}$, are considered in the communication link from node a to node b , Eq. (3) becomes:

$$y_k = \sqrt{P_{t,a}} \sqrt{G_{ab}} h_k x_k + n_k. \quad (13)$$

The average received Signal to Noise power Ratio (SNR) at node b is given by:

$$SNR_r = \frac{P_{t,a} E\{G_{ab}\} E\{h_k^2\} E\{|x_k|^2\}}{N_0} = \frac{P_{t,a} G_{ab}}{N_0}, \quad (14)$$

where $E\{h_k^2\} = 1$, $E\{|x_k|^2\} = 1$ and the received power at node b is given by $P_{t,a} E\{G_{ab}\} E\{h_k^2\} E\{|x_k|^2\}$. For ease of analysis, we define the ratio of the power transmitted from node a to the noise power encountered at the receiver of node b as the *transmit SNR*¹ [17] given by:

$$SNR_t = \frac{P_{t,a} E\{|x_k|^2\}}{N_0} = \frac{P_{t,a}}{N_0}. \quad (15)$$

Hence, we have:

$$\begin{aligned} SNR_r &= SNR_t G_{ab}, \\ \gamma_r &= \gamma_t + 10 \log_{10}(G_{ab}) \text{ [dB]}, \end{aligned} \quad (16)$$

where $\gamma_r = 10 \log_{10}(SNR_r)$ and $\gamma_t = 10 \log_{10}(SNR_t)$. Note that the effective receive power (or γ_r) at the RN and that at the DNs will be different when the corresponding communication links experience different RDRPLR. Therefore, it is not power-efficient, if the SN and RN use the same transmit power (or transmit SNR, γ_t), because not all communication links in Fig. 3 experience the same RDRPLR. In order to minimise the overall transmission power in the network, we also investigate an appropriately designed power sharing approach, where the SN and RN can use different transmit power levels, as long as the sum of them equals to the targeted average transmit power. Even when the SR and RD distance is identical, because the RN is

¹We note that this definition is based on measuring the signal power and noise power at different physical locations, but this unusual definition simplifies our discourse.

at the half way position, their propagation channels, physical-layer solutions and BER-requirements may be different. These differences underline the importance accurate power-sharing and control.

Let us denote the transmit SNR at SN_1 , SN_2 , RN, DN_1 and DN_2 as $\gamma_{t,S_1} = 10 \log_{10}(SNR_{t,S_1})$, $\gamma_{t,S_2} = 10 \log_{10}(SNR_{t,S_2})$, $\gamma_{t,R} = 10 \log_{10}(SNR_{t,R})$, $\gamma_{t,D_1} = 10 \log_{10}(SNR_{t,D_1})$ and $\gamma_{t,D_2} = 10 \log_{10}(SNR_{t,D_2})$, respectively. We also define the transmit SNR difference between SN_1 and RN, as well as that between SN_2 and RN as:

$$\begin{aligned} \Delta_{S_1R} &= \gamma_{t,S_1} - \gamma_{t,R} \\ 10 \log_{10}(\delta_{S_1R}) &= 10 \log_{10}(SNR_{t,S_1}/SNR_{t,R}), \end{aligned} \quad (17)$$

and

$$\begin{aligned} \Delta_{S_2R} &= \gamma_{t,S_2} - \gamma_{t,R} \\ 10 \log_{10}(\delta_{S_2R}) &= 10 \log_{10}(SNR_{t,S_2}/SNR_{t,R}), \end{aligned} \quad (18)$$

respectively. From Eqs. (17) and (18), we can compute the average transmit SNR as:

$$\begin{aligned} \overline{SNR}_t &= \frac{SNR_{t,S_1} + SNR_{t,S_2} + SNR_{t,R}}{3} \\ &= \frac{SNR_{t,R}(\delta_{S_1R} + \delta_{S_2R} + 1)}{3}. \end{aligned} \quad (19)$$

Hence, once we know the target average transmit SNR as well as δ_{S_1R} and δ_{S_2R} , we can compute the transmit SNR at the RN from:

$$SNR_{t,R} = \frac{3 \overline{SNR}_t}{\delta_{S_1R} + \delta_{S_2R} + 1}. \quad (20)$$

Similarly, we can determine the transmit SNR values at SN_1 and SN_2 from:

$$SNR_{t,S_1} = \frac{3 \overline{SNR}_t \delta_{S_1R}}{\delta_{S_1R} + \delta_{S_2R} + 1} \quad (21)$$

$$SNR_{t,S_2} = \frac{3 \overline{SNR}_t \delta_{S_2R}}{\delta_{S_1R} + \delta_{S_2R} + 1}. \quad (22)$$

Note that when no power sharing is employed, all nodes use the same transmit SNR, yielding $SNR_{t,S_1} = SNR_{t,S_2} = SNR_{t,R} = \overline{SNR}_t$.

The quantities Δ_{S_1R} and Δ_{S_2R} are determined based on the RN location and hence they are dependent on the corresponding RDRPLR factors. More specifically, Δ_{S_1R} is the difference of the RDRPLR factors between the RD_2 and S_1D_2 links:

$$\Delta_{S_1R} = 10 \log_{10}(G_{RD_2}) - 10 \log_{10}(G_{S_1D_2}). \quad (23)$$

Similarly, Δ_{S_2R} is the difference of the RDRPLR factors between the RD_1 and S_2D_1 links:

$$\Delta_{S_2R} = 10 \log_{10}(G_{RD_1}) - 10 \log_{10}(G_{S_2D_1}). \quad (24)$$

Note that we have $G_{S_1D_2} = G_{S_2D_1} = 2$ in the network topology shown in Fig. 1. Hence, when the RN is situated at location 'C' in Fig. 1, we have $\Delta_{S_1R} = \Delta_{S_2R} = 10 \log_{10}(4) - 10 \log_{10}(2) = 3$ dB. The Δ_{S_1R} and Δ_{S_2R} values corresponding to different locations are given in Table I.

Our aim is to make sure that the received SNR for the RD_1 (RD_2) link and that for the S_2D_1 (S_1D_2) link are always identical for any combinations of the RDRPLR values G_{RD_1} and $G_{S_2D_1}$ (G_{RD_2} and $G_{S_1D_2}$). The difference between the RDRPLR values is compensated by the assignment of different transmit power levels.

Modulation	16-StQAM, 16DPSK					
Mapping	Set Partitioning (SP)					
Coding	TC					
Constituent Code	Half-rate Recursive Systematic Convolutional (RSC) code					
Code Memory	2					
Outer iterations	2					
Inner TC iterations	4					
Decoder	Approximate Log-MAP					
Symbols per frame	1,200					
Number of frames	10,000					
Channel	Correlated Rayleigh fading channel having a normalised Doppler Frequency of 0.01					
RN Position:	G_{S_1R} (dB)	G_{S_2R} (dB)	G_{RD_1} (dB)	G_{RD_2} (dB)	Δ_{S_1R} (dB)	Δ_{S_2R} (dB)
A	9.03	9.03	2.04	2.04	-0.96	-0.96
B	8.06	8.06	3.91	3.91	0.91	0.91
C	6	6	6	6	3	3
D	3.91	3.91	8.06	8.06	5.06	5.06
E	2.04	2.04	9.03	9.03	6.03	6.03

TABLE I
SYSTEM PARAMETERS.

III. SIMULATION RESULTS

The performance of the 16-StQAM-TC and 16DPSK-TC schemes combined with the related NC schemes is investigated based on the simulation parameters of Table I.

Fig. 4 shows the Bit Error Ratio (BER) performance of the 16-StQAM-TC aided NC system, when employing RNs at different locations shown in Fig. 3, at a given SNR per bit of $E_b/N_0 = 13$ dB. When R is located at 'E', which is in the middle of DN_1 and DN_2 , the BER of the NC scheme without power sharing is the highest compared to other locations. As seen in Fig. 4, when the RN is located at 'C', which is in the centre of the butterfly-topology of Fig.3, the best BER performance is obtained for the scheme operating without power sharing. The dotted line illustrates the BER performance of the system invoking power sharing. It is worth noting that a RN situated at location 'D' would attain the best performance amongst the five locations considered in the presence of power sharing. This is because at location 'D' we have $d_{S_1R} \approx d_{S_1D_2}$, which means that the received SNR at the RN is almost identical to that at the DN_2 , when SN_1 broadcasts its signals to RN and DN_2 .

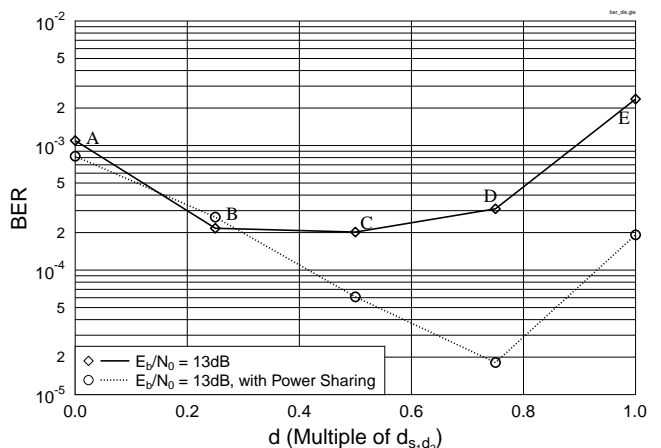


Fig. 4. BER performance in the case of $E_b/N_0 = 13$ dB with different RN position over correlated Rayleigh channels using system of Fig. 3 and simulation parameters of Table I.

Fig. 5 shows the BER versus E_b/N_0 performance of the proposed hybrid system, when communicating over correlated Rayleigh fading

channels. As seen in Fig. 5, the 16-StQAM-TC scheme outperforms the 16DPSK-TC arrangement by about 1.5 dB at a BER of 10^{-5} . This is mainly because the 16DPSK scheme has a lower minimum Euclidean distance between its adjacent constellation points than that of the 16-StQAM scheme. The 16-StQAM-TC assisted NC aided scheme operating without the power sharing mechanism outperforms the 16-StQAM-TC scheme by approximately 1.2 dB. When power sharing is used, the optimum RN location is closer to the DNs, so that $d_{S_1R} = d_{S_1D_2}$ and $d_{S_2R} = d_{S_2D_1}$, where the corresponding RDRPLR values are $G_{S_1R} = G_{S_2R} = 3$ dB and $G_{RD_1} = G_{RD_2} = 8.73$ dB. Another 1 dB of gain is attained by the power sharing based NC scheme. Similar trends can also be observed from the Frame Error Ratio (FER) versus E_b/N_0 performance curves seen in Fig. 6.

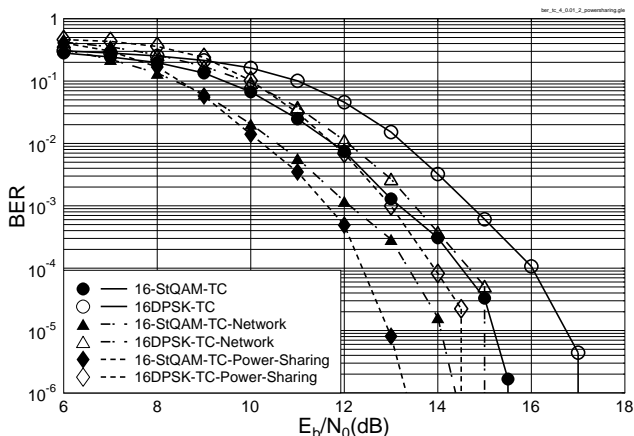


Fig. 5. BER versus E_b/N_0 performance for 16-StQAM and 16DPSK aided TC for transmission over Correlated Rayleigh channel using system of Fig. 1 and Fig. 3, simulation parameters of Table I.

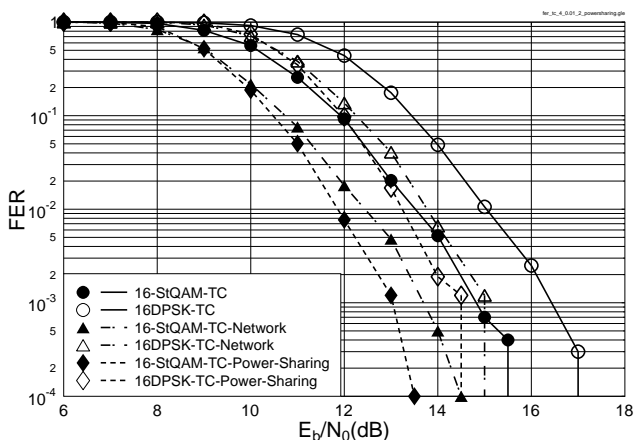


Fig. 6. FER versus E_b/N_0 performance for 16-StQAM and 16DPSK aided TC for transmission over Correlated Rayleigh channel using system of Fig. 1 and Fig. 3, simulation parameters of Table I.

IV. CONCLUSIONS

We have derived the symbol-to-bit soft-demapper LLR formulae for the 16-StQAM scheme and investigated its soft-decision aided performance in the context of a TC scheme. The 16-StQAM-TC scheme outperforms the similar throughput 16DPSK-TC scheme by about 1.5 dB at a BER of 10^{-5} , when communicating over correlated Rayleigh fading channels having a normalised Doppler frequency of 0.01.

We have also investigated a 16-StQAM-TC assisted NC scheme relying on a butterfly network topology. It was found that as expected,

the achievable BER performance is affected by the location of the RN. More specifically, when the transmit power at the SNs and RN are identical, the RN located at the centre of the butterfly network topology achieves the best performance. However, when the power sharing approach is invoked, the optimum RN location is closer to the DNs, where another 1 dB of power gain can be attained.

REFERENCES

- [1] E. Issman and W. Webb, "Carrier recovery for 16-level QAM in mobile radio," *IEE colloquium on multi-level modulation*, March 1990.
- [2] L. Hanzo, S. X. Ng, T. Keller, and W. Webb, *Quadrature Amplitude Modulation: From Basics to Adaptive Trellis-Coded, Turbo-Equalised and Space-Time Coded OFDM, CDMA and MC-CDMA Systems Digital Communications*. Wiley-IEEE Press, 2nd ed., 2004.
- [3] L. Chen, H. Kusaka, and M. Kominami, "Blind phase recovery in QAM communication systems using higher order statistics," *IEEE Signal Processing Letters*, vol. 3, pp. 147–149, May 1996.
- [4] W. Webb, L. Hanzo, and R. Steele, "Bandwidth-efficient QAM schemes for Rayleigh-fading channels," *IEE Proceedings Communications*, vol. 138, pp. 169–175, June 1991.
- [5] C.-D. Chung, "Differentially amplitude and phase-encoded QAM for the correlated Rayleigh-fading channel with diversity reception," *IEEE Transactions on Communications*, vol. 45, pp. 309–321, March 1997.
- [6] Y. Ma, Q. T. Zhang, R. Schober, and S. Pasupathy, "Diversity reception of dapsk over generalized fading channels," *IEEE Transactions on Wireless Communications*, vol. 4, pp. 1834–1846, July 2005.
- [7] D. Liang, S. X. Ng, and L. Hanzo, "Soft-decision Star-QAM aided BICM-ID," *Signal Processing Letters, IEEE*, vol. 18, no. 3, pp. 169–172, 2011.
- [8] C. Berrou and A. Glavieux and P. Thitimajshima, "Near Shannon limit error-correcting coding and decoding: Turbo codes," in *Proceedings of the International Conference on Communications*, (Geneva, Switzerland), pp. 1064–1070, May 1993.
- [9] R. Ahlswede, N. Cai, S.-Y. Li, and R. Yeung, "Network information flow," *IEEE Transactions on Information Theory*, vol. 46, pp. 1204–1216, Jul. 2000.
- [10] A. Sendonaris, E. Erkip, and B. Aazhang, "User cooperation diversity. Part I. system description," *IEEE Transactions on Communications*, vol. 51, pp. 1927–1938, Nov. 2003.
- [11] A. Sendonaris, E. Erkip, and B. Aazhang, "User cooperation diversity. Part II. implementation aspects and performance analysis," *IEEE Transactions on Communications*, vol. 51, pp. 1939–1948, Nov. 2003.
- [12] J.-Y. Hwang, J. Oh, J. Kim, and Y. Han, "Utility-aware network coding in wireless butterfly networks," in *Vehicular Technology Conference (VTC 2010-Spring)*, 2010 IEEE 71st, pp. 1–5, May 2010.
- [13] L. Hanzo, T. H. Liew, B. L. Yeap, R. Y. S. Tee, S. X. Ng, *Turbo Coding, Turbo Equalisation and Space-Time Coding: EXIT-Chart-Aided Near-Capacity Designs for Wireless Channels, 2nd Edition*. Wiley-IEEE Press, 2011.
- [14] S. ten Brink, "Convergence behaviour of iteratively decoded parallel concatenated codes," *IEEE Transactions on Communications*, vol. 49, pp. 1727–1737, October 2001.
- [15] J. Klierer, S. X. Ng, and L. Hanzo, "Efficient computation of EXIT functions for non-binary iterative decoding," *IEEE Transactions on Communications*, vol. 54, pp. 2133–2136, December 2006.
- [16] L. Hanzo and O. Alamri and N. El-Hajjar and N. Wu, *Near-Capacity Multi Functional MIMO Systems*. John Wiley & Sons, Ltd, May 2009.
- [17] H. Ochiai, P. Mitran, and V. Tarokh, "Design and analysis of collaborative diversity protocols for wireless sensor networks," in *IEEE Vehicular Technology Conference*, pp. 4645–4649, Sept. 2004.
- [18] S. X. Ng, Y. Li and L. Hanzo, "Distributed turbo trellis coded modulation for cooperative communications," in *IEEE ICC 2009*, (Dresden, Germany), pp. 1–5, 14–18 June 2009.